ARTICLE

Kinetically tuned dimensional augmentation as a versatile synthetic route towards robust metal–organic frameworks

Dawei Feng[1], Kecheng Wang[1], Zhangwen Wei[1], Ying-Pin Chen[1,2], Cory M. Simon[3], Ravi K. Arvapally[4], Richard L. Martin[5], Mathieu Bosch[1], Tian-Fu Liu[1], Stephen Fordham[1], Daqiang Yuan[6], Mohammad A. Omary[4], Maciej Haranczyk[5], Berend Smit[3,7] & Hong-Cai Zhou[1,2]

Metal–organic frameworks with high stability have been pursued for many years due to the sustainability requirement for practical applications. However, researchers have had great difficulty synthesizing chemically ultra-stable, highly porous metal–organic frameworks in the form of crystalline solids, especially as single crystals. Here we present a kinetically tuned dimensional augmentation synthetic route for the preparation of highly crystalline and extremely robust metal–organic frameworks with a preserved metal cluster core. Through this versatile synthetic route, we obtain large single crystals of 34 different iron-containing metal–organic frameworks. Among them, PCN-250(Fe_2Co) exhibits high volumetric uptake of hydrogen and methane, and is also stable in water and aqueous solutions with a wide range of pH values.

[1] Department of Chemistry, Texas A&M University, College Station, Texas 77843-3255, USA. [2] Department of Materials Science and Engineering, Texas A&M University, College Station, Texas 77842, USA. [3] Department of Chemical and Biomolecular Engineering, University of California at Berkeley, Berkeley, California 94720, USA. [4] Department of Chemistry, University of North Texas, Denton, Texas 76203, USA. [5] Computational Research Division, Lawrence Berkeley National Laboratory, One Cyclotron Road, MS 50F-1650, Berkeley, California 94720-8139, USA. [6] State Key Laboratory of Structural Chemistry, Fujian Institute of Research on the Structure of Matter, Chinese Academy of Sciences, Fujian, Fuzhou 350002, P. R. China. [7] Institut des Sciences et Ingénierie Chimiques, Ecole Polytechnique Fédérale de Lausanne (EPFL), CH-1015 Lausanne, Switzerland. Correspondence and requests for materials should be addressed to H.-C.Z. (email: zhou@chem.tamu.edu).

Metal–organic frameworks (MOFs) with good stability have been pursued for many years[1–4]. Chemically stable MOFs, which are resistant to reactive species, are of critical importance to a variety of applications, including gas storage, carbon capture, separations and catalysis[5–15]. In particular, robust MOFs that are easy to scale up and moisture-resistant with high gas storage capacity are needed for automotive applications. However, making robust MOFs with desired structure, porosity and internal surface properties has always been a challenge. Almost all MOFs, in particular moisture-resistant MOFs constructed with high-valence metal ions, have been made from the 'one-pot' synthetic route, making it difficult to control the metal-containing nodes and therefore the topology of the MOF[16].

Problems arise when targeting chemically stable MOFs through conventional one-pot reactions: The overall design of novel MOFs with expected structures, even simple functionalization of existing MOFs for targeted applications, becomes very challenging because of the unpredictable *in situ* formation of inorganic building blocks; mixed phases often come out together due to the formation of diverse inorganic building blocks; polycrystalline or even amorphous products are prone to form[17], which not only bring challenges in structure determination, but also influence the properties of the targeted products. To address these problems, we present a general method, which is derived from the rationalization of the MOF growth process from both a kinetic and a thermodynamic perspective, of synthesizing Fe-MOF single crystals with preformed inorganic building blocks [Fe$_2$M(μ_3-O)(CH$_3$COO)$_6$] (M = Fe$^{2+,3+}$, Co^{2+}, Ni^{2+}, Mn^{2+}, Zn^{2+}). Overall, we synthesize large single crystals of 34 different Fe-MOFs with thirty different ligands and mixed ligands by rationally tuning the synthetic conditions. Among them, PCN-250(Fe$_2$Co) (PCN stands for porous coordination network), which is stable in H$_2$O for more than 6 months, exhibits not only one of the highest total CH$_4$ uptakes of 200 V STP/V at 35 bar and 298 K, but also one of the highest total H$_2$ volumetric uptakes of 60 g L^{-1} at 40 bar and 77 K (refs 18,19).

Results

Rationalization of kinetics in the MOF growth process. Most chemically stable MOFs are constructed with hard Lewis acidic metal ions such as Fe^{3+}, Al^{3+} and Zr^{4+} when carboxylate ligands (hard bases) are used[20–25]. Due to the strong electrostatic interaction between the metal nodes and organic linkers, the frameworks are relatively resistant to the attack of H$_2$O and acidic or basic reactants. However, the stronger coordination bond is also more difficult to dissociate during the MOF growth process, which results in insufficient structure reorganization or defect reparation. As a result, highly crystalline stable MOFs are extremely difficult to synthesize under normal conditions.

The MOF crystal growth process is essentially ligand substitution on metal ions or clusters. As most substitution reactions of octahedral complexes go through a dissociative mechanism, ligand substitution reactions (X: initial coordinating ligand, L: bridging ligand) on each individual inorganic building block during MOF growth can be modelled as the stepwise substitution on metal or metal clusters (M; Supplementary Fig. 1)

The model in Supplementary Fig. 1 illustrates how we can tune the synthesis conditions to promote the flux of ligands on and off a metal cluster and hence facilitate defect reparation and structure reorganization. Consider a metal cluster fully bound to only initial coordinating ligands. The rate of substitution for one of the initial coordinating ligands with a bridging ligand (r_{s1})

$$r_{s1} = k_2[MX_5][L] \tag{1}$$

At steady state,

$$r_{s1} = \frac{k_2 k_1 [MX_6][L]}{k_{-1}[X] + k_2[L]} \tag{2}$$

Thus, **X** behaves as a competitor to L, and we can slow the rate of bridging ligand attachment by increasing the concentration of **X**. For the dissociation process of the bridging ligand, the reaction rate is

$$r_{d1} = k_{-2}[MX_5L] \qquad \left(k_i = Ae^{-\frac{E_a}{RT}}\right) \tag{3}$$

For relatively soft Lewis acidic species such as Cu^{2+} and Zn^{2+}, interactions with hard basic carboxylates are relatively weak, so the activation energy E_a for the dissociation process is small, which yields a large k_{-2} and a fast dissociation process. Meanwhile, the excess of solvent molecules could serve as an **X** ligand to compete with the bridging ligand **L**, which slows down the ligand substitution process. Consequently, ligand substitution and dissociation rates are comparable, allowing sufficient structure reorganization and defect reparation to form long-range ordered structures under moderate conditions.

For hard Lewis acidic species such as Fe^{3+}, Al^{3+} and Zr^{4+}, their strong electrostatic interaction with the hard basic carboxylate gives rise to a much larger E_a and smaller k_{-2}. Even if solvent molecules act as an **X** ligand, the much larger k_1 value still causes unbalanced substitution and dissociation reaction rates. As a result, direct synthesis of those MOFs usually results in a long-range disordered (amorphous) product due to the lack of structural reorganization. Since E_a is determined by the nature of the metal and the coordinating ligand, increasing the synthetic temperature **T** is an approach to raise k_{-2} and facilitate the ligand dissociation process. Unfortunately, higher temperatures also accelerate the substitution process and an unbalanced substitution–dissociation process still exists. To accelerate the ligand dissociation process at higher temperature and maintain a slow ligand substitution process, an extra competing reagent **X**, which binds more strongly to the metal (smaller k_1) than the solvent molecule is necessary. With the assistance from the extra competing reagent **X**, reversible ligand rearrangement could be tuned to facilitate the crystallization process[26,27]. Because it is actually the carboxylate and not the acid doing the substitution, when the deprotonation process is taken into account, extra acetic acid could simultaneously inhibit the deprotonation of the ligand, which further slows down the substitution reaction and aids the crystallization process.

Simplification of MOFs growth using preformed [Fe$_2$M(μ_3-O)(CH$_3$COO)$_6$]. As M$_3$(μ_3-O)(COO)$_6$ (M = Fe, Cr, Al, Sc, V, In) is one of the most common building blocks in the reported trivalent metal species containing MOFs[28], to test our hypothesis, we used [Fe$_2$M(μ_3-O)(CH$_3$COO)$_6$] as the starting material and acetic acid (acetate after deprotonation) as the competing reagent to grow Fe-MOFs with many different ligands (Supplementary Methods). [Fe$_2$M(μ_3-O)(CH$_3$COO)$_6$] as isolated basic carboxylates have been reported for decades[29]. Excellent solubility of these clusters increases their feasibility as a starting material. Meanwhile, due to the strong electrostatic interaction between Fe^{3+} and μ_3-O^{2-}, the cluster is inherently robust enough to preserve the integrity of the core while going through carboxylate substitution on the periphery under solvothermal conditions. Moreover, the D_{3h} cluster itself possesses six carboxylate arms in a trigonal prismatic arrangement, which allows facile construction of three-dimensional frameworks through simple bridging. When [Fe$_2$M(μ_3-O)(CH$_3$COO)$_6$] is used as a starting material, direct synthesis of Fe-MOFs can be considered as a pure ligand substitution process and the framework growth can be

rationalized by a traditional stepwise ligand substitution reaction model (Supplementary Methods). Therefore, the addition of extra competing reagent can tune both ligand substitution and dissociation processes directly via concentration variation.

Consequently, with the assistance of acetic acid as a competing reagent, we obtained large single crystals of 34 Fe-MOFs containing the [Fe$_2$M(μ_3-O)] building block (Supplementary

Data 1, Supplementary Figs 2–36, Supplementary Tables 1–31, Supplementary Note 1).

Discussion

Even though the ligands shown in Fig. 1b vary in symmetry, functionality, connectivity and size, the structure of the [Fe$_2$M(μ_3-
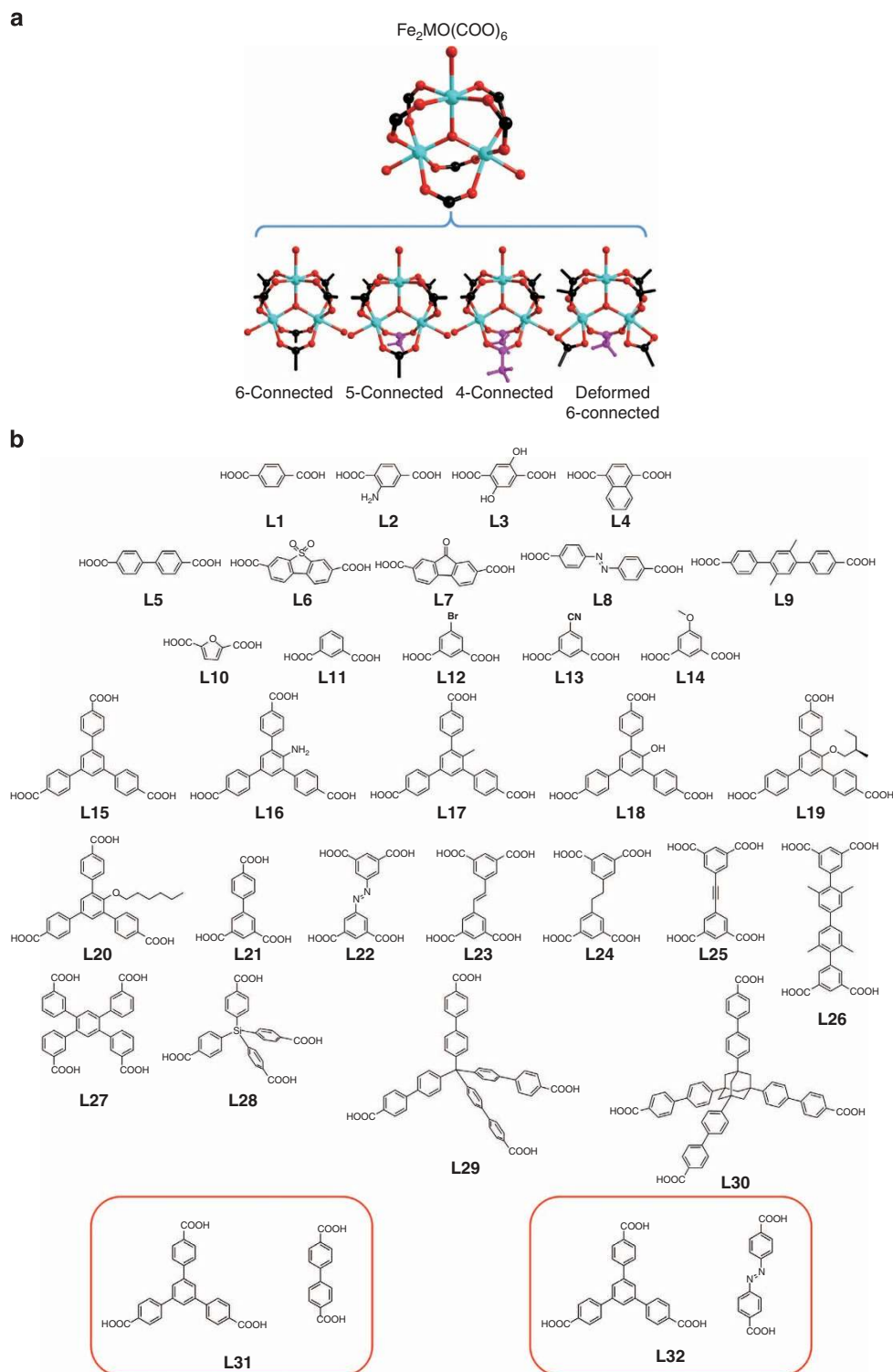

Figure 1 | Organic linkers used and different connecting modes. (a) Four different connecting modes of the [Fe$_2$M(μ_3-O)] cluster. Carboxylates on ligands and terminal acetates are represented by black and purple, respectively. **(b)** Thirty different ligands and two types of mixed ligands used in constructing Fe-MOFs.

O)] building block is maintained in these frameworks. Thus, the new synthetic strategy can be viewed as a dimensional augmentation process from zero-dimensional metal-containing nodes of $[Fe_2M(\mu_3\text{-}O)]$ to three-dimensional nets. Partial substitution on the $[Fe_2M(\mu_3\text{-}O)]$ clusters has also occurred when complete substitution becomes incompatible with some of the ligands because of symmetry requirements or steric hindrance.

To demonstrate our versatility of the kinetically tuned dimensional augmentation strategy, MOFs with distinct structural features are discussed in detail.

PCN-240, constructed from **L3**, is isostructural to MIL-88 with the acs-a topology (Fig. 2a)[3]. Usually, **L3** tends to form the MOF-74 structure with two hydroxyl groups participating in coordination. However, when starting from $[Fe_2M(\mu_3\text{-}O)(COOCH_3)_6]$, the *in situ* formation of the one-dimensional

chain can be avoided and only a simple substitution reaction occurs between carboxylates, leaving two hydroxyl groups free for other potential modifications. With elongated ligands **L5** and **L9**, which allows sufficient space for catenation, twofold perpendicular interpenetration and threefold parallel interpenetration have been observed, respectively. Interestingly, the interpenetration restricts the flexibility in each single net and therefore stabilizes the framework and generates permanent porosity (Fig. 2a). The mixed ligand strategy is challenging due to the high probability of obtaining mixed phases, especially for MOFs on the basif of high-valence metals whose structure determination relied almost exclusively on powder X-ray diffraction. When starting with pre-assembled metal clusters, the interference from side reactions generating different inorganic building blocks is eliminated. The mixed ligand MOFs can be more easily synthesized with the kinetically tuned dimensional augmentation strategy, which allows for growing single crystals instead of powders. Using the combinations of **L15** and **L5**, as well as **L15** and **L8**, we obtained large single crystals of PCN-280 and PCN-285 (Fig. 2b).
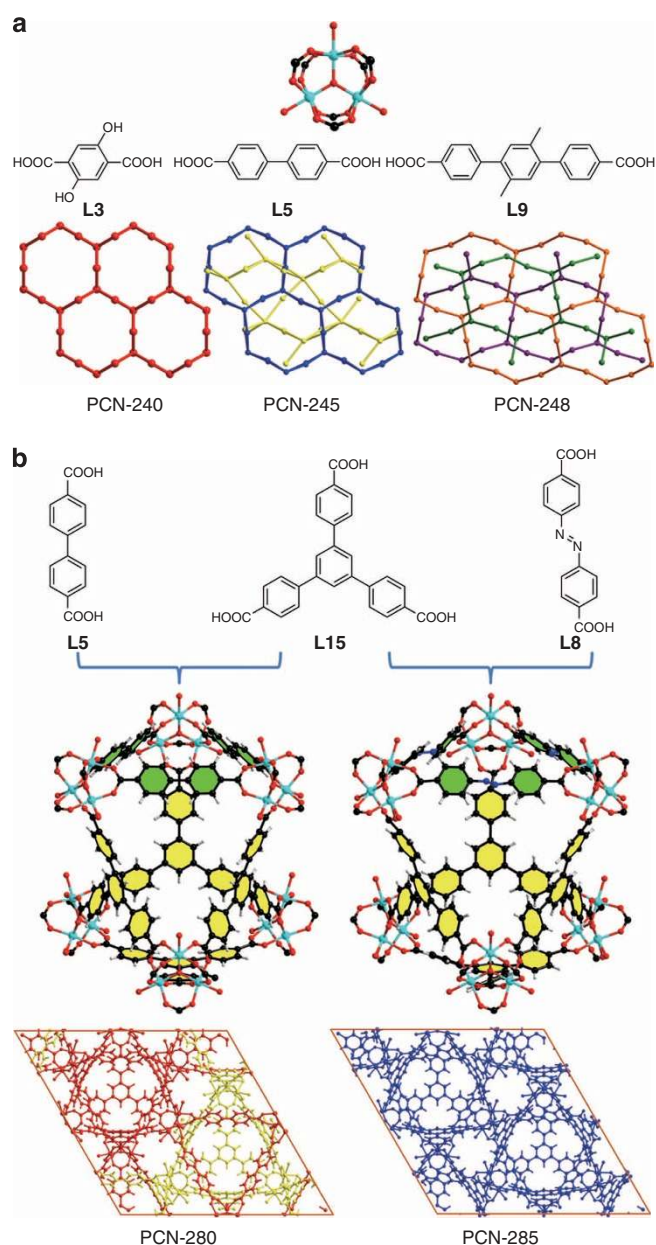
Figure 2 | Functionalization and mixed ligands in Fe-MOFs.
(**a**) Functionalized MIL-88 isostructure, 2-fold and 3-fold self-interpenetration. (**b**) PCN-280(interpenetrated) and PCN-285(non-interpenetrated) constructed from mixed ligands.
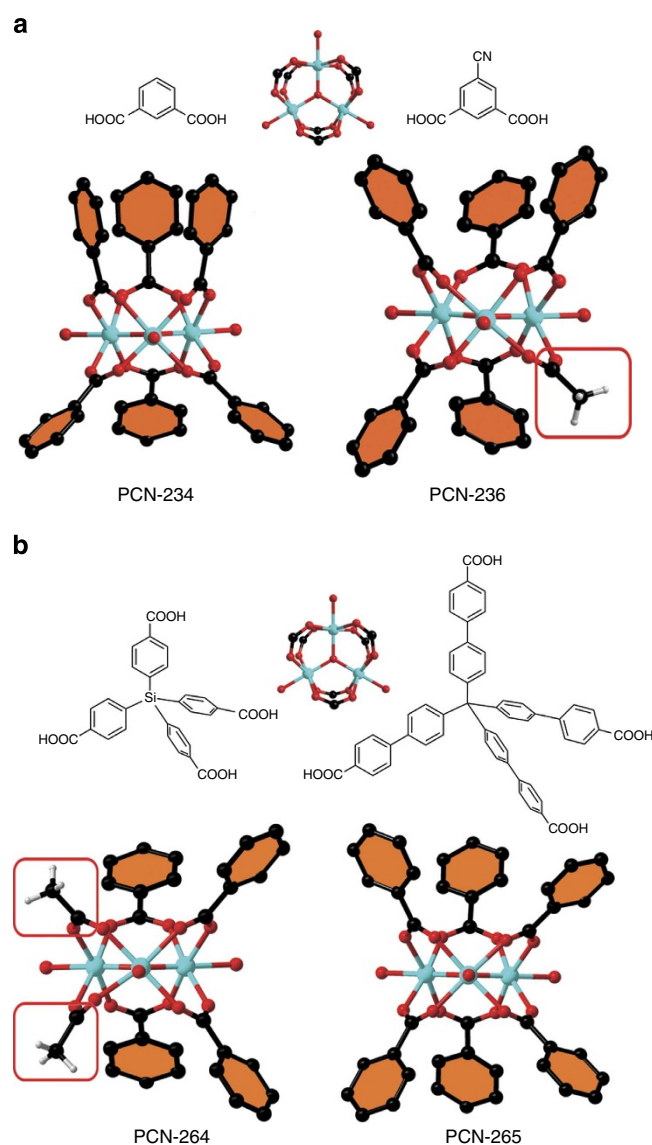

Figure 3 | Partially substituted $[Fe_2M(\mu_3\text{-}O)]$ in Fe-MOFs. (**a**) Bulky group induced partial substitution in PCN-236. (**b**) Rigidity induced partial substitution in PCN-264.

PCN-234 is isostructural to MIL-59 with the CaB$_6$ net (Fig. 3a)[30]. When the ligand is functionalized by bulky groups like -CN, the limited distance between each ligand prevents complete substitution on the [Fe$_2$M(μ$_3$-O)] cluster and forces the

formation of a 5-connected cluster with acetic acid as the remaining terminal ligand (Fig. 3b), giving rise to PCN-236. This connectivity reduction also occurs with the tetrahedral ligands: in PCN-265, **L29** slightly stretches from the ideal T_d symmetry to D_{2d} symmetry to form a 6-connected [Fe$_2$M(μ$_3$-O)]-containing framework, while the smaller tetrahedral ligand **L28** is too rigid to bend and maintains the original T_d symmetry in PCN-264. Complete substitution on the [Fe$_2$M(μ$_3$-O)] core is unable to form a long-range ordered structure with T_d symmetric **L28**, so the connectivity of the [Fe$_2$M(μ$_3$-O)] cluster is reduced to four (Fig. 3c). This reduced connectivity on the [Fe$_2$M(μ$_3$-O)] cluster is first discovered here in these Fe-MOFs, which is also an evidence of the substitution reaction of the preformed basic carboxylate.

Although all the Fe-MOFs are synthesized under similar conditions, the optimal concentration of acetic acid for each one varies greatly. According to our rationalization, extra acetic acid should slow down the substitution reaction rate, which shows the kinetic influence. When the concentration of acetic acid was much lower than the optimal value, gels or amorphous products were obtained, which suggests insufficient control of the substitution and dissociation balance (Supplementary Methods). When the concentration of acetic acid is too high, solutions remain clear with no solid products even after a long period, which suggests a thermodynamic equilibrium in the solution. If MOF formation is expressed as an equilibrium (Supplementary Fig. 37) and the formation of clear solution is treated as the point of a positive Gibbs free energy, then the amount of acetic acid is actually an indication of relative values for the framework's free energy of formation. The entropic effects can be clearly observed from the synthetic conditions (Supplementary Table 32). For ligands with similar size and connectivity, MOFs containing Fe$_2$MO clusters with lower connectivity always need a lower concentration of acetic acid as the competing reagent. Meanwhile, for Fe$_2$MO clusters with the same connectivity, ligands with higher connecting numbers always need more acetic acid. Assuming these MOFs have similar enthalpies of formation, the concentration change of acetic acid is consistent with the entropy change. Moreover, even if the connectivity of clusters and ligands are the same, the amount of acetic acid for those MOFs still varies (Supplementary Table 33), which could be attributed to an enthalpic effect (Supplementary Methods).

Methane uptake is highly related to the structure of the porous material used[19]. Because of the structural diversity of the Fe-MOFs synthesized by us, we turned to computational methods to quickly predict their methane uptake (Supplementary Methods, Supplementary Figs 44–47). In addition, we utilize an *in silico* approach to predict a set of new structures and their methane uptake (Supplementary Data 2 and Supplementary Methods). Figure 4a shows the simulated deliverable capacities of our predicted structures and those structures that have been synthesized together with the experimental data of PCN-250(Fe$_3$) and PCN-250(Fe$_2$Co). Our simulations suggest that PCN-250 is indeed an outlying structure for vehicular methane

a

b

c

d

PCN-250   PCN-250′

e

PCN-250(Fe2Co)

f

g

h
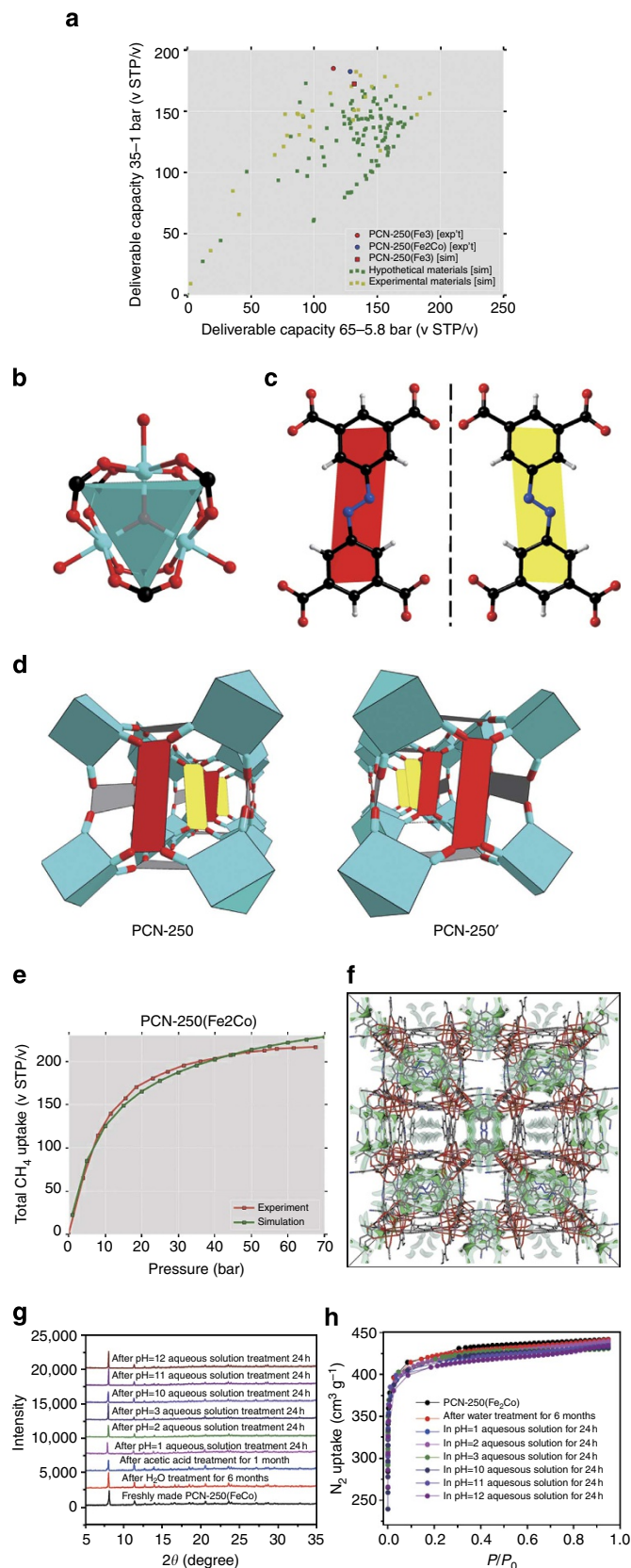
Figure 4 | Simulated and experimental CH$_4$ adsorption of Fe-MOFs.
(**a**) Performance plot of deliverable capacities using two different pressure swings. Shown are the predictions for the Fe-MOFs synthesized here (yellow) and *in silico* predicted structures (green). Red and blue points show PCN-250. Our predicted crystal structures and molecular simulation results can be found in the Supplementary Data 1 and 2. (**b**–**d**) Structures of PCN-250 and PCN-250′. (**e**) Total CH$_4$ adsorption uptake of PCN-250 at 298 K and (**f**) contours of the computed potential energy surface of adsorbed CH$_4$ in PCN-250. (**g**) Powder X-ray patterns and (**h**) N$_2$ adsorption isotherms of PCN-250(Fe$_2$Co) after stability tests.

storage using a 35–1 bar pressure swing. Interestingly, our screening predicts that several of the synthesized Fe-MOFs have very high deliverable capacities using a 65–5.8 bar pressure swing. Also, our simulations confirm that PCN-250 has the highest 35 bar loading of all structures considered in this analysis (Supplementary Figs 42 and 43).

PCN-250 consists of 6-connected [$Fe_2M(\mu_3$-O)] building blocks and rectangular tetratopic **L22** (Fig. 4b–d), which is isostructural to the reported indium MOF[31]. Interestingly, PCN-250′, another framework isomer of PCN-250, is found under different synthetic conditions (Supplementary Methods). Along one axis, ligands constructing the same cube in PCN-250 adopt mirror configurations and are alternatively arranged. In PCN-250′, ligands adopt the same configuration in the one cube and mirror configuration in the adjacent cubes along any axis. Experimental results show PCN-250(Fe_2Co) that possesses total CH_4 uptake of 200 v/v at 35 bar and 298 K (Fig. 4e), which is one of the highest among all the reported MOFs. PCN-250(Fe_2Co) has a record high H_2 uptake of 3.07 wt% and 28 g L^{-1} at 1.2 bar and 77 K (Supplementary Fig. 38). It also has one of the highest total volumetric H_2 uptakes, 60 g L^{-1} (Supplementary Fig. 41), at high pressure due to its high crystal density.

Both high uptake of H_2 and CH_4 can be attributed to suitable size of the cage in PCN-250 and the well-dispersed, highly charged open metal sites (Fig. 4f). Each cube in PCN-250 is faced by **L22** and the channels between each cube are surrounded by high valent open metal sites. Therefore, all of the void space is provided with adsorption sites, which can strongly interact with both H_2 and CH_4 molecules. This results in efficient space utilization to reach a high volumetric uptake and leads to an induced polarization of gas molecules by high-valence metal cations through charge-induced dipole interaction. This high-valence metal ion and induced dipole interaction can polarize additional layers of gas molecules, allowing multiple layers of gas to adsorb without significant drop in the adsorption enthalpy. The heat of adsorption is relatively low compared with a single-site adsorption by orbital interaction, such as the Kubas binding of hydrogen molecules. However, it is far-reaching, making it nearly flat over a wide range of uptakes (Supplementary Figs 39 and 40, Supplementary Methods).

Even after the insertion of the softer Lewis acid M(II) in the μ_3-oxo trimmer, the PCN-250 series still shows extraordinary chemical stability. The powder patterns of PCN-250(Fe_2Co) remained unaltered upon immersion in glacial acetic acid and pH = 1 to pH = 11 aqueous solutions for 24 h (Fig. 4g,h). The framework of PCN-250(Fe_2Co) remained stable under H_2O after 6 months (Fig. 4g,h, Supplementary Tables 34 and 35). Moreover, the N_2 adsorption isotherms of PCN-250(Fe_2Co) remain constant after all these treatments, which suggest no phase transition or framework decomposition during all the treatments. A combination of high uptake and chemical stability is quite rare for MOFs, and this combination can guarantee the reusability of the sorbent for industrial applications. With its high gas uptake, extraordinary stability and excellent scalability, PCN-250 is a viable candidate for natural gas storage for automotive applications.

Methods
Preparation of preformed clusters. $Fe_2M(\mu_3$-O) $(CH_3COO)_6$ (abbreviated to Fe_2M in MOFs' syntheses) (M = Mn, Co, Ni, Zn) is prepared according to reported procedure[25]:

A solution of sodium acetate trihydrate (42 g, 0.31 mol) in water (70 ml) was added to a filtered, stirred solution of iron(III) nitrate nonahydrate (8 g, 0.02 mol) and the metal(II) nitrate (0.1 mol) in water 70 ml, and the brown precipitate was filtered off, washed with water and with ethanol and dried in air. For M = Zn, the total volume of water used in the preparation was restricted to 70 ml and a red-brown precipitate appeared overnight.

Synthesis of PCN-233. **L10** (15 mg), Fe_2Co (15 mg) and acetic acid (0.4 ml) in 2 ml of N,N-dimethyl formamide (DMF) were ultrasonically dissolved in a Pyrex vial. The mixture was heated in an oven at 120 °C for 12 h. After cooling down to room temperature, dark brown crystals were collected by filtration.

Synthesis of PCN-234. **L11** (8 mg), Fe_3 (15 mg) and acetic acid (0.4 ml) in 2 ml of H_2O were ultrasonically dissolved in a Pyrex vial. The mixture was heated in an oven at 120 °C for 12 h. After cooling down to room temperature, dark brown crystals were collected by filtration.

Synthesis of PCN-235. **L11** (15 mg), Fe_2Co (15 mg) and acetic acid (0.2 ml) in 2 ml of DMF were ultrasonically dissolved in a Pyrex vial. The mixture was heated in an oven at 150 °C for 24 h. After cooling down to room temperature, dark brown crystals were collected by filtration.

Synthesis of PCN-236. **L13** (15 mg), Fe_2Co (15 mg) and acetic acid (0.1 ml) in 2 ml of DMF were ultrasonically dissolved in a Pyrex vial. The mixture was heated in an oven at 150 °C for 12 h. After cooling down to room temperature, dark brown crystals were collected by filtration.

Synthesis of PCN-237. **L12** (15 mg), Fe_2Co (15 mg) and acetic acid (0.2 ml) in 2 ml of N-methyl pyrrolidone (NMP) were ultrasonically dissolved in a Pyrex vial. The mixture was heated in an oven at 150 °C for 12 h. After cooling down to room temperature, dark brown crystals were collected by filtration.

Synthesis of PCN-238. **L14** (15 mg), Fe_2Co (15 mg) and acetic acid (0.1 ml) in 2 ml of NMP were ultrasonically dissolved in a Pyrex vial. The mixture was heated in an oven at 150 °C for 12 h. After cooling down to room temperature, dark brown crystals were collected by filtration.

Synthesis of PCN-240. **L3** (10 mg), Fe_2Co (10 mg) and acetic acid (0.25 ml) in 2 ml of N,N-diethylformamide and H_2O (v/v = 1/1) were ultrasonically dissolved in a Pyrex vial. The mixture was heated in an oven at 150 °C for 24 h. After cooling down to room temperature, dark brown crystals were collected by filtration.

Synthesis of PCN-241. **L4** (10 mg), Fe_2Co (15 mg) and acetic acid (0.8 ml) in 2 ml of DMF were ultrasonically dissolved in a Pyrex vial. The mixture was heated in an oven at 150 °C for 12 h. After cooling down to room temperature, dark brown crystals were collected by filtration.

Synthesis of PCN-242. **L2** (10 mg), Fe_3 (10 mg) and acetic acid (0.45 ml) in 2 ml of DMF were ultrasonically dissolved in a Pyrex vial. The mixture was heated in an oven at 150 °C for 12 h. After cooling down to room temperature, dark brown crystals were collected by filtration.

Synthesis of PCN-243. **L8** (10 mg), Fe_3 (10 mg) and acetic acid (0.45 ml) in 2 ml of DMF were ultrasonically dissolved in a Pyrex vial. The mixture was heated in an oven at 150 °C for 48 h. After cooling down to room temperature, dark brown crystals were collected by filtration.

Synthesis of PCN-245. **L5** (10 mg), Fe_3 (10 mg) and acetic acid (0.15 ml) in 2 ml of DMF were ultrasonically dissolved in a Pyrex vial. The mixture was heated in an oven at 150 °C for 12 h. After cooling down to room temperature, dark brown crystals were collected by filtration.

Synthesis of PCN-246. **L7** (10 mg), Fe_3 (15 mg) and acetic acid (0.2 ml) in 2 ml of DMF were ultrasonically dissolved in a Pyrex vial. The mixture was heated in an oven at 120 °C for 12 h. After cooling down to room temperature, dark brown crystals were collected by filtration.

Synthesis of PCN-247. **L6** (10 mg), Fe_3 (15 mg) and acetic acid (0.35 ml) in 2 ml of DMF were ultrasonically dissolved in a Pyrex vial. The mixture was heated in an oven at 150 °C for 12 h. After cooling down to room temperature, dark brown crystals were collected by filtration.

Synthesis of PCN-248. **L9** (10 mg), Fe_2Co or Fe_3 (10 mg) and acetic acid (0.25 ml) in 2 ml of NMP were ultrasonically dissolved in a Pyrex vial. The mixture was heated in an oven at 150 °C for 24 h. After cooling down to room temperature, dark brown crystals were collected by filtration.

Synthesis of PCN-250. **L22** (10 mg), Fe_2M (Mn, Fe, Co, Ni, Zn) (15 mg) and acetic acid (1 ml) in 2 ml of DMF were ultrasonically dissolved in a Pyrex vial.

The mixture was heated in an oven at 140 °C for 12 h. After cooling down to room temperature, dark brown crystals were collected by filtration.

Large scale synthesis of PCN-250. L22 (1 g), Fe₂M (Mn, Fe, Co, Ni, Zn,) (1 g) and acetic acid (100 ml) in 200 ml of DMF were ultrasonically dissolved in a 500 ml Pyrex bottle. The mixture was heated in an oven at 140 °C for 12 h. After cooling down to room temperature, dark brown crystals were collected by filtration.

Synthesis of PCN-250′. L22 (10 mg), Fe₂M (Mn, Fe, Co, Ni, Zn) (15 mg) and acetic acid (1 ml) in 2 ml of NMP were ultrasonically dissolved in a Pyrex vial. The mixture was heated in an oven at 140 °C for 12 h. After cooling down to room temperature, dark brown crystals were collected by filtration.

Synthesis of PCN-251. L22 (10 mg), Fe₂M (Mn, Fe, Co, Ni, Zn) (15 mg) and acetic acid (1 ml) in 2 ml of NMP were ultrasonically dissolved in a Pyrex vial. The mixture was heated in an oven at 140 °C for 12 h. After cooling down to room temperature, dark brown crystals were obtained.

Synthesis of PCN252. L23 (10 mg), Fe₂M (Mn, Fe, Co, Ni, Zn) (10 mg) and acetic acid (0.8 ml) in 2 ml of NMP were ultrasonically dissolved in a Pyrex vial. The mixture was heated in an oven at 150 °C for 12 h. After cooling down to room temperature, dark brown crystals were colllected by filtration.

Synthesis of PCN-253. L24 (10 mg), Fe2M (Mn, Fe, Co, Ni, Zn,) (15 mg) and acetic acid (1 ml) in 2 ml of NMP were ultrasonically dissolved in a Pyrex vial. The mixture was heated in an oven at 150 °C for 12 h. After cooling down to room temperature, dark brown crystals were collected by filtration.

Synthesis of PCN-254. L25 (10 mg), Fe₂M (Mn, Fe, Co, Ni, Zn) (15 mg) and acetic acid (1 ml) in 2 ml of NMP were ultrasonically dissolved in a Pyrex vial. The mixture was heated in an oven at 150 °C for 12 h. After cooling down to room temperature, dark brown crystals were collected by filtration.

Synthesis of PCN-255. L26 (10 mg), Fe₂Co (15 mg) and acetic acid (0.5 ml) in 2 ml of NMP were ultrasonically dissolved in a Pyrex vial. The mixture was heated in an oven at 150 °C for 12 h. After cooling down to room temperature, dark brown crystals were collected by filtration.

Synthesis of PCN-256. L27 (10 mg), Fe₂Co (15 mg) and acetic acid (0.4 ml) in 2 ml of NMP and 0.1 ml n-pentanol were ultrasonically dissolved in a Pyrex vial. The mixture was heated in an oven at 150 °C for 12 h. After cooling down to room temperature, dark brown crystals were collected by filtration.

Synthesis of PCN-257. L21 (10 mg), Fe₃ (15 mg) and acetic acid (0.4 ml) in 2 ml of NMP and 0.1 ml n-pentanol were ultrasonically dissolved in a Pyrex vial. The mixture was heated in an oven at 150 °C for 12 h. After cooling down to room temperature, dark brown crystals were collected by filtration.

Synthesis of PCN-260. L15 (15 mg), Fe₂Co (5 mg) and acetic acid (0.25 ml) in 2 ml of NMP were ultrasonically dissolved in a Pyrex vial. The mixture was heated in an oven at 150 °C for 24 h. After cooling down to room temperature, dark brown crystals were collected by filtration.

Synthesis of PCN-261-NH₂. L16 (15 mg), Fe₂Co (15 mg) and acetic acid (0.22 ml) in 2 ml of DMF were ultrasonically dissolved in a Pyrex vial. The mixture was heated in an oven at 150 °C for 12 h. After cooling down to room temperature, dark brown crystals were collected by filtration.

Synthesis of PCN-261-CH₃. L17 (15 mg), Fe₂Co (15 mg) and acetic acid (0.2 ml) in 2 ml of DMF were ultrasonically dissolved in a Pyrex vial. The mixture was heated in an oven at 150 °C for 12 h. After cooling down to room temperature, dark brown crystals were collected by filtration.

Synthesis of PCN-261-Chiral. L19 (15 mg), Fe₂Co (15 mg) and acetic acid (0.2 ml) in 2 ml of DMF were ultrasonically dissolved in a Pyrex vial. The mixture was heated in an oven at 150 °C for 12 h. After cooling down to room temperature, dark brown crystals were collected by filtration.

Synthesis of PCN-262. L18 (10 mg), Fe₂Ni (10 mg) and acetic acid (0.25 ml) in 2 ml of DMF were ultrasonically dissolved in a Pyrex vial. The mixture was heated in an oven at 150 °C for 12 h. After cooling down to room temperature, dark brown crystals were collected by filtration.

Synthesis of PCN-263. L20 (10 mg), Fe₂Ni (10 mg) and acetic acid (0.3 ml) in 2 ml of DMF were ultrasonically dissolved in a Pyrex vial. The mixture was heated in an oven at 150 °C for 73 h. After cooling down to room temperature, dark brown crystals were collected by filtration.

Synthesis of PCN-264. L28 (10 mg), Fe₃ (10 mg) and acetic acid (0.6 ml) in 2 ml of DMF were ultrasonically dissolved in a Pyrex vial. The mixture was heated in an oven at 150 °C for 24 h. After cooling down to room temperature, dark brown crystals were collected by filtration (Yield 80%).

Synthesis of PCN-265. L29 (10 mg), Fe₂Ni (15 mg) and acetic acid (0.43 ml) in 2 ml of DMF were ultrasonically dissolved in a Pyrex vial. The mixture was heated in an oven at 150 °C for 12 h. After cooling down to room temperature, dark brown crystals were collected by filtration.

Synthesis of PCN-266. L30 (10 mg), Fe₃ (15 mg) and acetic acid (0.3 ml) in 2 ml of DMF were ultrasonically dissolved in a Pyrex vial. The mixture was heated in an oven at 150 °C for 12 h. After cooling down to room temperature, dark brown crystals were collected by filtration.

Synthesis of PCN-280. L5 (10 mg), L15 (10 mg), Fe₃ (10 mg) and acetic acid (0.2 ml) in 2 ml of NMP and 0.1 ml n-pentanol were ultrasonically dissolved in a Pyrex vial. The mixture was heated in an oven at 150 °C for 12 h. After cooling down to room temperature, dark brown crystals were collected by filtration.

Synthesis of PCN-285. L8 (10 mg) and L15 (10 mg), Fe₃ (10 mg) and acetic acid (0.2 ml) in 2 ml of NMP and 0.1 ml n-pentanol were ultrasonically dissolved in a Pyrex vial. The mixture was heated in an oven at 150 °C for 12 h. After cooling down to room temperature, dark brown crystals were collected by filtration.

MIL-88 synthesis. BDC (10 mg), Fe₂Co or Fe₃ (10 mg) NMP 2 ml and acetic acid (0.2 ml) were ultrasonically dissolved in a Pyrex vial. The mixture was heated in an oven at 150 °C for 12 h. After cooling down to room temperature, dark brown crystals were collected by filtration.

References

1. Zhou, H.-C., Yaghi, O. M. & Long, J. R. Introduction to metal–organic frameworks. *Chem. Rev.* **112,** 673–674 (2012).
2. Férey, G. *et al.* A chromium terephthalate-based solid with unusually large pore volumes and surface area. *Science* **309,** 2040–2042 (2005).
3. Serre, C. *et al.* Role of solvent–host interactions that lead to very large swelling of hybrid frameworks. *Science* **315,** 1828–1831 (2007).
4. Banerjee, R. *et al.* High-throughput synthesis of zeolitic imidazolate frameworks and application to CO2 capture. *Science* **319,** 939–943 (2008).
5. Kitagawa, S., Kitaura, R. & Noro, S. Functional porous coordination polymers. *Angew. Chem. Int. Ed.* **43,** 2334–2375 (2004).
6. Herm, Z. R. *et al.* Separation of hexane isomers in a metal-organic framework with triangular channels. *Science* **340,** 960–964 (2013).
7. Deng, H. *et al.* Large-pore apertures in a series of metal-organic frameworks. *Science* **336,** 1021–1023 (2012).
8. Bloch, E. D. *et al.* Hydrocarbon separations in a metal-organic framework with open iron(II) coordination sites. *Science* **335,** 1606–1610 (2012).
9. Farha, O. K. *et al. De novo* synthesis of a metal–organic framework material featuring ultrahigh surface area and gas storage capacities. *Nat. Chem.* **2,** 944–948 (2010).
10. Cavka, J. H. *et al.* A new zirconium inorganic building brick forming metal organic frameworks with exceptional stability. *J. Am. Chem. Soc.* **130,** 13850–13851 (2008).
11. Férey, G. *et al.* A hybrid solid with giant pores prepared by a combination of targeted chemistry, simulation, and powder diffraction. *Angew. Chem. Int. Ed.* **43,** 6296–6301 (2004).
12. Surblé, S. *et al.* A new isoreticular class of metal-organic-frameworks with the MIL-88 topology. *Chem. Commun.* **3,** 284–286 (2006).
13. Dincă, M. *et al.* Hydrogen storage in a microporous metal–organic framework with exposed Mn²⁺ coordination sites. *J. Am. Chem. Soc.* **128,** 16876–16883 (2006).
14. Li, J.-R., Sculley, J. & Zhou, H.-C. Metal–organic frameworks for separations. *Chem. Rev.* **112,** 869–932 (2012).
15. Yoon, M., Srirambalaji, R. & Kim, K. Homochiral metal–organic frameworks for asymmetric heterogeneous catalysis. *Chem. Rev.* **112,** 1196–1231 (2012).
16. Tranchemontagne, D. J., Mendoza-Corte's, J. L., O'Keeffe, M. & Yaghi, O. M. Secondary building units, nets and bonding in the chemistry of metal–organic frameworks. *Chem. Soc. Rev.* **38,** 1257–1283 (2009).
17. Li, L. *et al.* A synthetic route to ultralight hierarchically micro/mesoporous Al(III)-carboxylate metal-organic aerogels. *Nat. Commun.* **4,** 1774 (2013).

7

18. Murray, L. J., Dincă, M. & Long, J. R. Hydrogen storage in metal–organic frameworks. *Chem. Soc. Rev.* **38,** 1294–1314 (2009).
19. Makal, T. A., Li, J.-R., Lu, W. & Zhou, H.-C. Methane storage in advanced porous materials. *Chem. Soc. Rev.* **41,** 7761–7779 (2012).
20. Yang, S. *et al.* Selectivity and direct visualization of carbon dioxide and sulfur dioxide in a decorated porous host. *Nat. Chem.* **4,** 887–894 (2012).
21. Yuan, D. *et al.* Stepwise adsorption in a mesoporous metal–organic framework: experimental and computational analysis. *Chem. Commun.* **48,** 3297–3299 (2012).
22. Chevreau, H. *et al.* Mixed-linker hybrid superpolyhedra for the production of a series of large-pore iron(III) carboxylate metal–organic frameworks. *Angew. Chem. Int. Ed.* **52,** 5056–5060 (2013).
23. Dan-Hardi, M. *et al.* A new photoactive crystalline highly porous titanium(IV) dicarboxylate. *J. Am. Chem. Soc.* **131,** 10857–10859 (2009).
24. Serre, C. *et al.* A route to the synthesis of trivalent transition-metal porous carboxylates with trimeric secondary building units. *Angew. Chem. Int. Ed.* **43,** 6285–6289 (2004).
25. Guillerm, V. *et al.* A zirconium methacrylate oxocluster as precursor for the low-temperature synthesis of porous zirconium(IV) dicarboxylates. *Chem. Commun.* **46,** 767–769 (2010).
26. Shimomura, S. *et al.* Flexibility of porous coordination polymers strongly linked to selective sorption mechanism. *Chem. Mater.* **22,** 4129–4131 (2010).
27. Schaate, A. *et al.* Modulated synthesis of Zr-based metal–organic frameworks: from nano to single crystals. *Chem. Eur. J.* **17,** 6643–6651 (2011).
28. Schoedel, A. & Zaworotko, M. J. [M$_3$(μ_3-O)(O$_2$CR)$_6$] and related trigonal prisms: versatile molecular building blocks for crystal engineering of metal–organic material platforms. *Chem. Sci.* **5,** 1269–1282 (2014).
29. Blake, A. B. *et al.* Magnetic and spectroscopic properties of some heterotrinuclear basic acetates of chromium(III), iron(III), and divalent metal ions. *J. Chem. Soc. Dalton Trans.* **12,** 2509–2520 (1985).
30. Barthelet, K. *et al.* [VIII(H$_2$O)]$_3$O(O$_2$CC$_6$H$_4$CO$_2$)3 · (Cl, 9H$_2$O) (MIL-59): a rare example of vanadocarboxylate with a magnetically frustrated three-dimensional hybrid framework. *Chem. Commun.* 1492–1493 (2002).
31. Liu, Y. *et al.* Assembly of metal–organic frameworks (MOFs) based on indium-trimer building blocks: a porous MOF with soc topology and high hydrogen storage. *Angew. Chem. Int. Ed.* **46,** 3278–3283 (2007).

Author contributions

D.F., K.W. and H.-C.Z. planned and executed the synthesis and characterization. Z.W. and Y.-P.C. analysed the single-crystal X-ray diffraction data. R.K.A., M.A.O. and D.Y. performed the high pressure adsorption measurement. C.M.S., R.L.M., B.S. and M.H. performed the gas adsorption calculation and simulation. M.B., T.-F.L. and S.F. performed the ICP analysis and ligand synthesis. All the authors participated in the preparation of the manuscript.

Corrigendum: Kinetically tuned dimensional augmentation as a versatile synthetic route towards robust metal–organic frameworks

Dawei Feng, Kecheng Wang, Zhangwen Wei, Ying-Pin Chen, Cory M. Simon, Ravi K. Arvapally, Richard L. Martin, Mathieu Bosch, Tian-Fu Liu, Stephen Fordham, Daqiang Yuan, Mohammad A. Omary, Maciej Haranczyk, Berend Smit & Hong-Cai Zhou